Journal of Membrane Science 640 (2021) 119804

Contents lists available at ScienceDirect

Journal of Membrane Science

journal homepage: www.elsevier.com/locate/memsci

A high ion-conductive and stable porous membrane for neutral aqueous Zn-based flow batteries

Yuyue Zhao [1], Pengyang Xiang [1], Ying Wang, Xiao Sun, Daxian Cao, Hongli Zhu *

Department of Mechanical and Industrial Engineering, Northeastern University, 360 Huntington Avenue, Boston, MA, 02115, USA

ARTICLE INFO

Keywords:
Non-solvent induced phase separation
Porous ion conducting membrane
High ion conductivity
Excellent stability
Zn-based flow batteries

ABSTRACT

Zn-based flow batteries (ZFBs) with low cost and high efficiency have become one of promising energy storage technologies for renewable energy development. However, in ZFBs, an anion exchange membrane (AEM) losses ion conductivity because of the presence of Zn^{2+}. The side reaction of Zn^{2+} precipitation resulted in ion exchange decomposition of AEM with quaternary groups. While a cation exchange membrane (CEM) hinders anion conductivity because of electrostatic interaction between ion-exchange groups and anions. To address poor ion conductivity of ion exchange membrane in ZFBs, a polyetherimide (PEI)-based porous ion conductive membrane is developed via water phase inversion technology for ZFBs. The ion conductive mechanism is based on pore size exclusion, which mitigates the effects of ion exchange groups on ion conductivity. The membrane performance is further improved by introducing suitable polyvinylpyrrolidone (PVP) and controlling tetrahydrofuran (THF) volatilization time. The results demonstrate that in Zn/4-Hydroxy-2,2,6,6-tetramethyl-piperidine 1-Oxyl (TEMPO-OH) flow battery, a coulombic efficiency (CE) of more than 98% and an energy efficiency (EE) of ~77% was achieved at 20 mA cm^{-2}, and the flow battery assembled with 20PEI-1PVP-90s can stably run for 150 cycles. The PEI-based porous membrane with low cost and high efficiency is considered as a promising strategy for ZFBs.

1. Introduction

The development of energy technology is changing human lifestyles and promoting the social progress. However, limiting fossil energy resources cannot meet long-term sustainable development goals. Meanwhile, environmental issues from consumption of fossil fuels affect the global environment and ecological balance. Therefore, a new energy revolution – the renewable energy revolution is taking place globally, including solar energy, wind power, hydropower, and other new technologies. However, power output of renewable energy is intermittent, unstable and uncontrollable because of the weather, illumination, season, and other objective factors, so the development of renewable energy is essential as a support for energy storage systems [1,2]. Aqueous flow battery is becoming one of promising large-scale energy storage technologies to develop renewable resources owing to their characteristic of decoupling of capacity and power, long life time and high safety [3,4]. Especially, aqueous Zn-based flow batteries (ZFBs) are becoming one of outstanding applications because of low cost, low redox potential of zinc (−0.76 V vs. Standard Hydrogen Electrode) and elimination of electrolyte volume [5–7].

A membrane plays a crucial role in preventing battery short and transferring ions to complete the current loop in a flow battery [8–10]. Currently, one of the ion conducting membranes widely used in flow batteries is the perfluorinated ion exchange membrane, such as Nafion 115 [11]. In general, the Nafion 115 membrane exhibits high ion conductivity and stability, but poor ion selectivity, leading to battery capacity fast fade during long-term cycling test [12,13]. In addition, its high expense significantly inhibits its large-scale application in flow batteries. Non-perfluorinated ion exchange membranes exhibit excellent ion conductivity and selectivity in flow batteries, while poor chemical stability hardly meets the request for long time application, especially in harsh atmospheres [14]. In ZFBs, an anion exchange membrane (AEM) should be employed as a membrane, which transfers anions and balances charges during cycling proceedings [15]. However, the presence of Zn^{2+} ions resulted in the decomposition of quaternary functional groups, such as the trimethylammonium groups [16]. Consequently, the presence of Zn^{2+} dramatically decreases ion conductivity of AEM. Meanwhile, a cation exchange membrane (CEM) hinders negative ions

* Corresponding author.
E-mail address: h.zhu@neu.edu (H. Zhu).
[1] Equal contribution.

https://doi.org/10.1016/j.memsci.2021.119804
Received 20 July 2021; Received in revised form 24 August 2021; Accepted 25 August 2021
Available online 1 September 2021

conductivity due to electrostatic interaction (Donnan effect).

In order to address the above-mentioned challenges, the porous ion conducting membrane has been studied, in which the ion transport is based on pore size exclusion mechanism [17,18]. The porous membrane prepared via conventional water phase inversion method possessed asymmetric finger-like pores structure and a skin layer, which plays a crucial role in various ions selectivity. Due to the complexity of porous membrane morphologies tunability, the flow battery performance varies considerably. The introduction of additives and different non-solvent enables to impact membrane microstructures [19]. The morphologies of porous membrane can be tuned by introducing polyvinylpyrrolidone (PVP) in a cast solution, in which more porous structure and continuity of pore structure can be formed to promote ion conductivity [20]. The various morphologies of porous membranes can be formed by tuning the composition of non-solvent bath as well. The polyvinylidene fluoride (PVDF) porous membrane fabricated in water/ethanol dual-coagulation bath showed morphological changes from figure-like asymmetric porous structure to spherical particle symmetric structure accompanying macro-voids disappearance [21].

Recently, the pore morphologies of porous membrane have been further investigated by adjusting the diffusion between solvents and non-solvents, the composition of non-solvent phase during non-solvent induced phase separation (NIPS). The morphologies of prepared porous membrane can be tuned by using different non-solvents. For poly ether sulfone/sulfonated poly (ether ether ketone) (PES/SPEEK) composite polymer solution, a thick and relative hydrophobic skin layer with narrow slits, and hydrophilic porous support layer were formed during NIPS, where the skin layer with slits inhibited active materials crossover and the hydrophilic porous structures promoted proton transportation through membrane [22]. The controllable porous structures in a porous membrane enabled to be realized by regulating the internal and external solvent diffusion rates [23]. A thin and dense selective layer was formed in the mixed non-solvent atmosphere owing to extra-fast internal diffusion between the casting solution and non-solvent, and a porous support layer was fabricated in the water-phase by NIPS. Therefore, to achieve a membrane with high selectivity and ionic conductivity, developing an effective way to control and tune the morphology of membranes is inevitable, and then further boosts flow battery performance.

In this work, a porous membrane based on polyetherimide (PEI) was fabricated by conventional NIPS technologies, and the morphologies of porous membrane enabled to be adjusted by introducing hydrophilic polymer additive and volatilizing co-solvent (tetrahydrofuran, THF). PEI is an amorphous thermoplastic with good chemical and thermal stability, which provides excellent calendar life in neutral aqueous ZFBs. Different from conventional ion exchange membrane, the porous ion conducting membrane transports ions through pore size exclusion mechanism, which minimizes the effect of ion exchange groups on membrane performance. The introduction of PVP improved membrane hydrophilicity and increased the pore size and connectivity, which promoted ion conductivity through the membrane. The addition of volatilizing THF can promote the formation of a dense skin layer by controlling volatilization time before phase inversion process, which improves ion selectivity. As a result, the PEI-based porous membrane could achieve good ion conductivity and excellent selectivity by optimizing the amount of PVP and THF evaporation time.

2. Results and discussion

A series of PEI-based porous ion conducting membranes with various PVP ratios and THF volatilization time was prepared via the water phase inversion technology and applied in neutral aqueous Zn/4-Hydroxy-

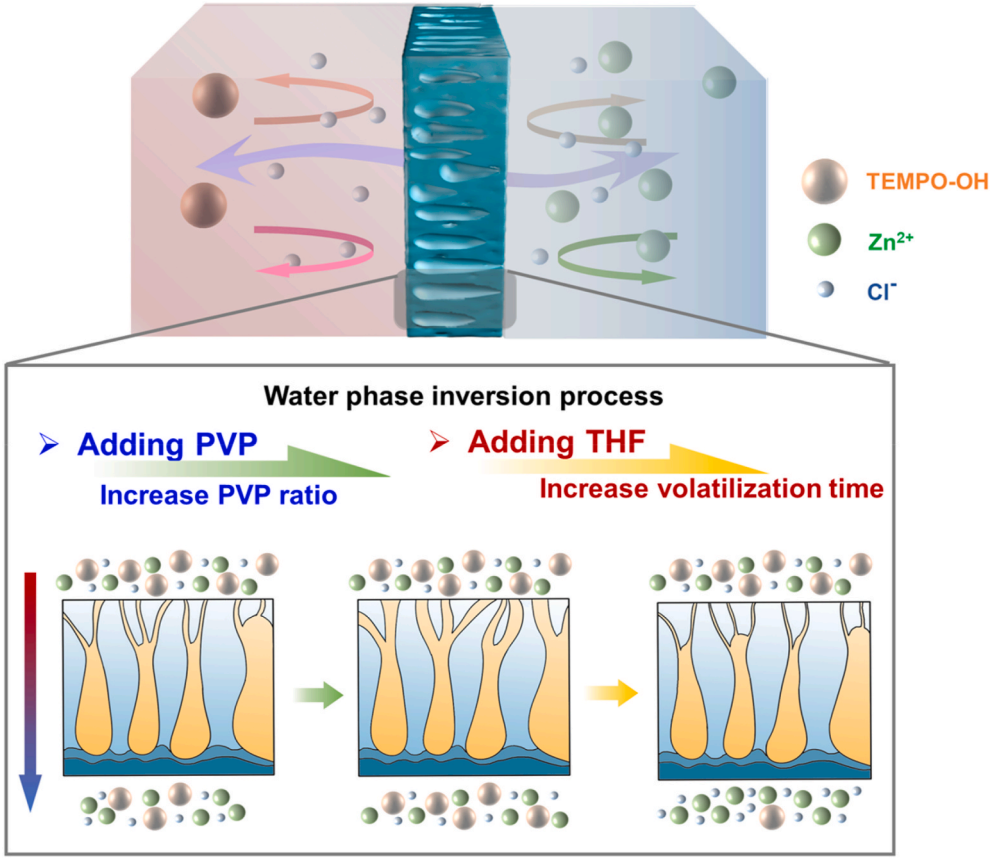

Fig. 1. The scheme of PEI-based porous ion conducting membrane application in neutral aqueous Zn/TEMPO-OH flow battery and membrane morphologies adjustment mechanism: the introduction of PVP promotes pore size and volatilization time of co-solvent (THF) decreases pore size of skin layer.

2,2,6,6-tetramethyl-piperidine 1-Oxyl (TEMPO-OH) flow battery (See Fig. 1). The morphology of porous membrane could be further adjusted and controlled by adding PVP in a cast solution and volatilizing THF before phase inversion, then adjusted battery performance. The pore size and continuity of pore structure are enhanced by introducing various amounts of PVP, which encourages ion conductivity but hinders membrane selectivity. The volatilization time of cast solution before phase inversion facilitates to form a dense skin layer, enhancing membrane selectivity.

The effect of additive and co-solvent volatilization on the pore structure of PEI-based porous membranes was observed via SEM (See Fig. 2 and Fig. S1). As presented in Fig. 2 (a) and (b), the pristine PEI porous ion conducting membrane exhibited a finger-like support in the cross-section structure and a dense upper surface morphology, which was determined by thermodynamic and kinetic factors of conventional water phase inversion process. In Fig. 2 (c), the sponge-like pore structure was observed on the pore wall. The PVP was introduced in the cast solution to tune the morphologies of PEI-based membranes.

In general, the introduction of PVP in a cast solution increased the viscosity and reduced the miscibility of polymer solutions with non-solvent, which promoted thermodynamic process and hindered kinetic process during water-phase inversion process [24]. As demonstrated in Fig. 2 (d), (e) and (f), with the increasing amount of PVP from 1.2%wt to 3.6%wt (Table 1), the larger pores and more macro-void were formed. The thickness of skin-layer tended to reduce, which was beneficial to improve ion conductivity. Compared with pristine PEI porous membrane, the wide distribution of island-shaped pores on the surface can be observed via SEM in Fig. S1. The pore distribution on the surface tended to be more intensive due to the increase of PVP in cast solutions, which benefited ion conductivity across porous membrane. Apparently, in this case, the thermodynamic enhancement dominated the phase inversion process. The addition of PVP promoted thermodynamic properties during phase separation process. The hydrophilicity of polymer solution enhanced exchange between solvent and non-solvents during the demixing process [25].

The morphologies of porous membranes were further tuned by adding THF as co-solvent and controlling volatilization time before phase separation, in which the surface polymer concentration of casting membrane was concentrated due to THF volatilization. Fig. 2(g–i) exhibited that the delayed demixing resulted in a denser skin layer on the surface of 20PEI/1PVP-z due to the THF vocalization, where z was 30s, 60s and 90s, respectively, and stood for the volatilization time. With the volatilization time increasing, the denser upper surfaces were formed, shown in Fig. 1S (d-f). These results were favorable to improve membrane selectivity.

The physicochemical properties of fabricated porous membranes, including contact angle, area resistance, water uptake, swelling ratio, and porosity, were further characterized to investigate influence of membrane structures. As listed in Table 1, the thickness of prepared membranes was about 110 ± 3 μm, which is a little thinner than that of Nafion 115 (132 ± 5 μm). The introduction of hydrophilic PVP significantly improved membrane hydrophilicity. As displayed in Fig. 3(a–d), the contact angles of PEI-based porous membranes decreased from 68.85° to 45.45° due to the increasing amount of hydrophilic PVP and more porous surface, which is much lower than that of Nafion 115 (87.56°, shown in Fig. 3 (h)). The contact angle of 20PEI/1PVP-z membranes, shown in Fig. 3(e–g), increased from 60.48° to 70.03°, which was explained by the formation of smoother surface

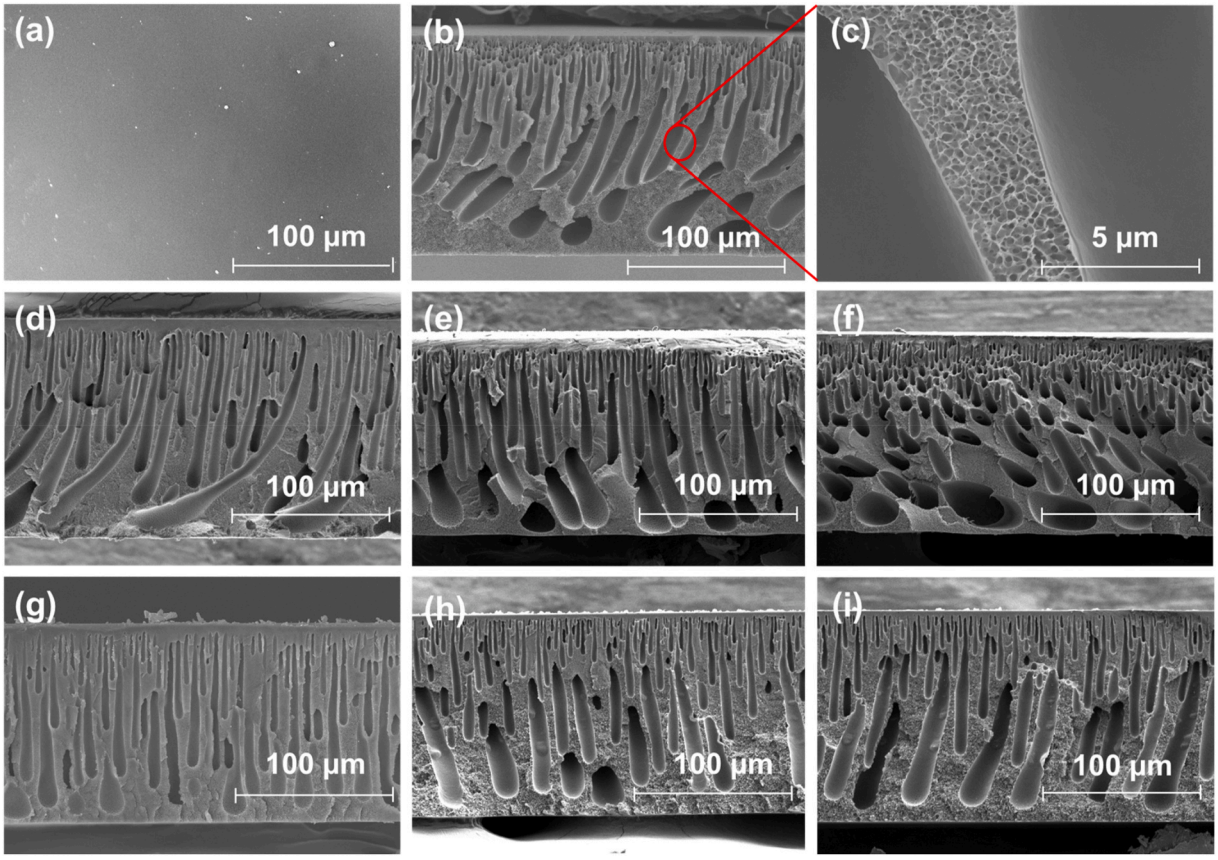

Fig. 2. The morphologies of various PEI-based porous membranes: (a–c) the surface and cross-section of pristine PEI porous membrane: (a) the surface toward glass plate, (b) the cross-section, (c) the magnified pore well; (d–f) cross-section morphologies of PEI-based porous membranes with different PVP ratios: (d) 20PEI/1PVP, (e) 19PEI/2PVP, (f) 18PEI/3PVP; (g–i) the cross-section morphologies of 20PEI/1PVP with different volatilization time: (g) 20PEI/1PVP-30s, (h) 20PEI/1PVP-60s, (i) 20PEI/1PVP-90s.

Table 1
Physicochemical properties of Nafion 115 and PEI-based porous membranes.

Membrane	Proportion (PEI/PVP/NMP/THF)	THF hold time (s)	Thickness (μm)	Water uptake (%)	Porosity (%)	Swelling Ratio (%)
Nafion 115	NA	NA	132 (±5)	15.0	NA	2.1
PEI	2.1/0/6.3/0	NA	109 (±5)	147.0	56.0	1.5
20PEI/1PVP	2.0/0.1/6.3/0	NA	108 (±5)	177.9	67.8	5.8
19PEI/2PVP	1.9/0.2/6.3/0	NA	110 (±5)	213.5	75.4	6.1
18PEI/3PVP	1.8/0.3/6.3/0	NA	113 (±5)	240.9	81.7	6.8
20PEI/1PVP-30s	2.0/0.1/6.3/5.67	30	110 (±15)	187.3	68.7	5.1
20PEI/1PVP-60s	2.0/0.1/6.3/5.67	60	107 (±5)	174.6	60.8	2.6
20PEI/1PVP-90s	2.0/0.1/6.3/5.67	90	112 (±5)	165.6	57.5	1.8

Note that the membrane name of xPEI/yPVP-z, where x, y and z were the weight ratios of PEI and PVP, and the volatilization time, respectively.

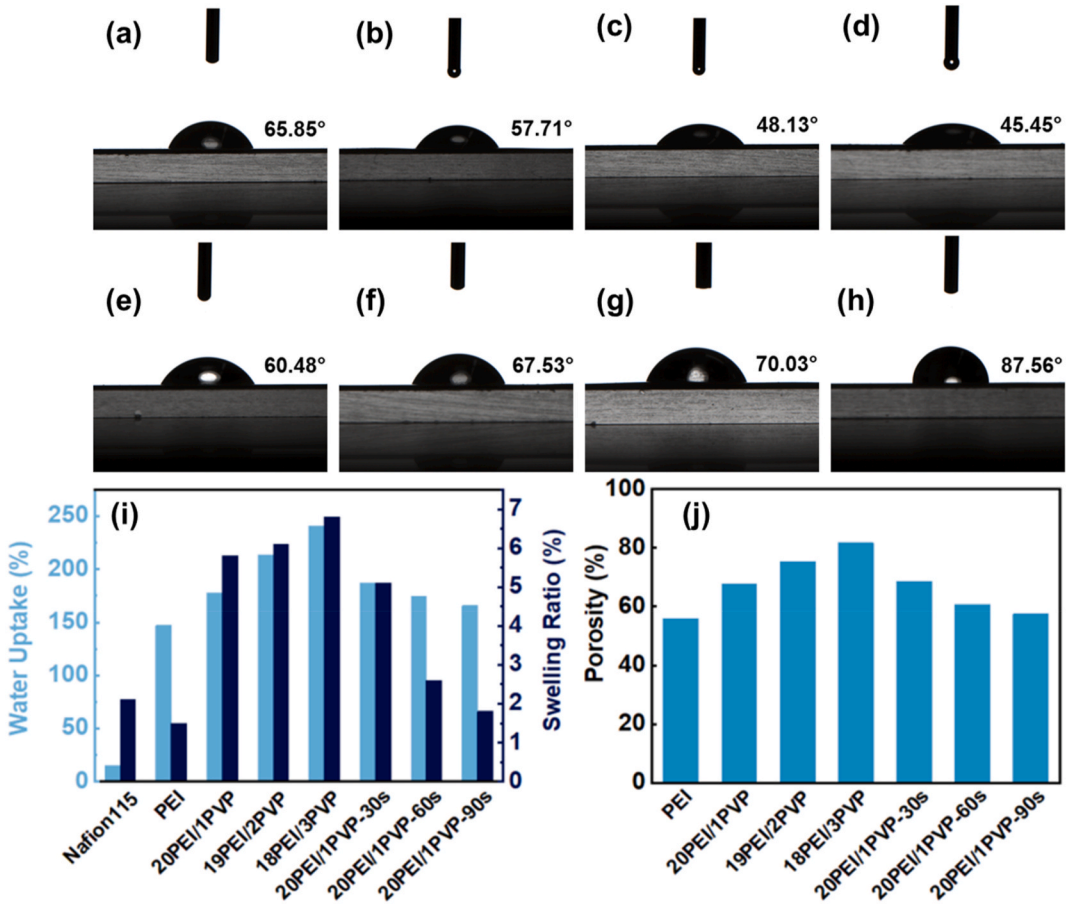

Fig. 3. The contact angle of Nafion 115 and various PEI-based porous membranes: (a) pristine PEI, (b) 20PEI/1PVP, (c) 19PEI/2PVP, (d) 18PEI/3PVP, (e) 20PEI/1PVP-30s, (f) 20PEI/1PVP-60s, (g) 20PEI/1PVP-90s, (h) Nafion 115; (i) The water uptake and swelling ratio of Nafion 115 and various PEI-based porous membranes; (j)The porosity of various PEI-based porous membranes.

morphologies. The contact angle of hydrophilic porous membranes mildly increased because of various surface roughness [26]. On the hydrophilic surface, the increasing roughness tends to achieve apparently decreased contact angle [26]. Meanwhile, the water uptake and swelling ratio of PEI-based membranes showed gradually enhancing tendency with the increase of PVP (See Fig. 3 (i)). The addition of PVP is favorable to form more porous structures, which resulted in higher water uptake. The 18PEI/3PVP showed the maximum water uptake of more than 240%, demonstrating that more electrolyte can be absorbed in the porous membrane to promote ion transportation, but hindered membrane selectivity. The swelling ratio of the prepared membrane slightly increased from 1.5% to 6.1%, which indicated good dimensional stability. As shown in Fig. 3 (j), the porosity of xPEI/yPVP membranes exhibited an increasing tendency as well. While with increasing volatilization time, the porosity of 20PEI/1PVP-z membrane decreased.

To further link porous structures with their ion conductivity and selectivity, the membrane area resistance and permeability of TEMPO-OH were characterized and shown in Fig. 4(a–c). Fig. 4 (a) showed the area resistance of Nafion 115 and PEI-based porous membrane in 1 M NH_4Cl electrolyte. The area resistance of 20PEI/1PVP porous membrane (0.73 Ω cm^2) was comparable to Nafion 115 (0.60 Ω cm^2). With the increase of PVP ratio, the area resistance of xPEI/yPVP membrane were reduced from 0.73 Ω cm^2 to 0.30 Ω cm^2 owing to the formation of more connective porous structures and more hydrophilicity, which was much lower than that of initial PEI porous membrane (8.36 Ω cm^2). While the 20PEI/1PVP-z membranes with different volatilization time exhibited gradually increasing area resistance (from 0.80 Ω cm^2 to 0.85 Ω cm^2). The 20PEI/1PVP-90s (0.85 Ω cm^2) exhibited comparable area resistance value to 20PEI/1PVP membrane (0.73 Ω cm^2). As shown in Fig. 4 (b), the ionic conductivity of PEI-based membrane increased from

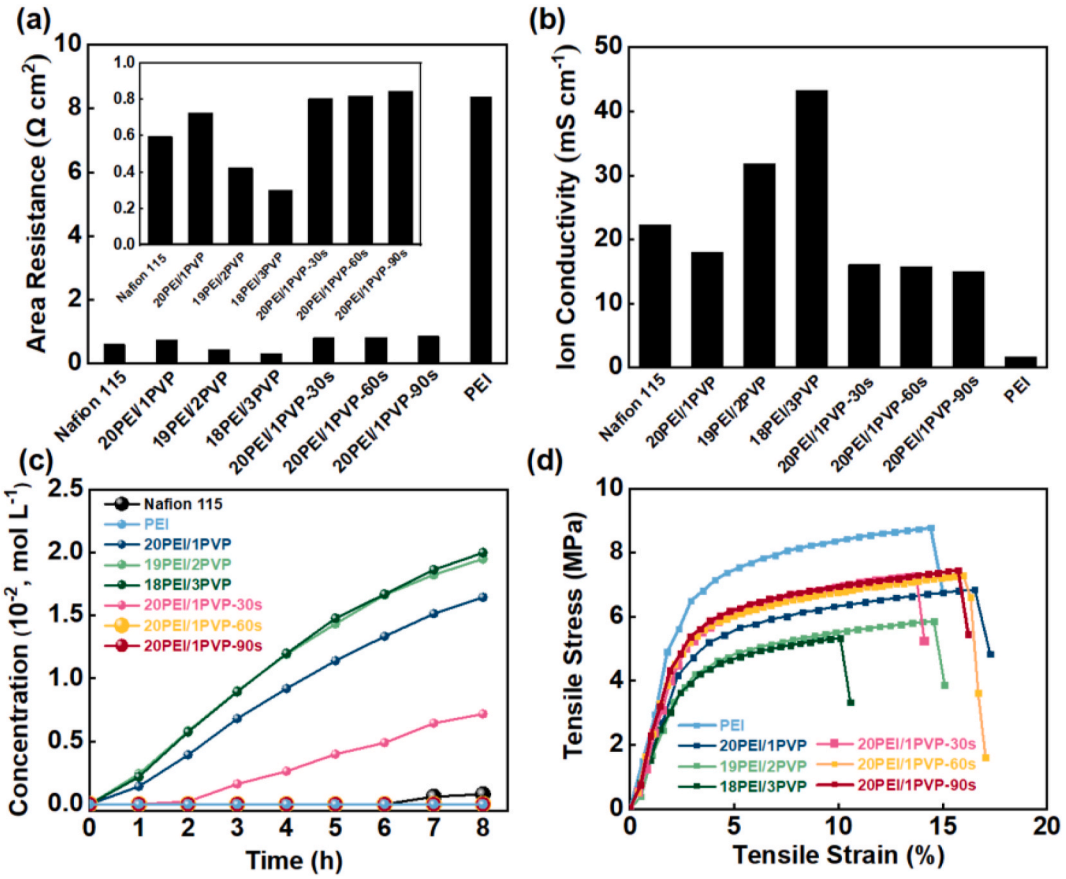

Fig. 4. (a) the area resistance of Nafion 115 and various PEI-based porous membranes (The insert is locally zoomed-in area resistance.), (b) The ion conductivity of Nafion 115 and various PEI-based porous membranes, (c) the TEMPO-OH permeability of Nafion 115 and various PEI-based porous membranes, (d) Stress vs. strain curves for various PEI-based porous membranes.

18.0 mS cm^{-1} to 43.2 mS cm^{-1} with the amount of PVP increasing, indicating that the introduction of PVP was beneficial to enhance ion transportation. The corresponding ion conductivities of 20PEI/1PVP-z membranes slightly decreased. The ion conductivities of 20PEI/1PVP-90s membranes was 15 mS cm^{-1}, which is comparable to 20PEI/1PVP (18 mS cm^{-1}). Different from Nafion 115, the homemade porous membranes presented in this work enable to transport different ions through membrane. The ion selectivity of PEI-based porous membranes was measured and described in Fig. 4 (c). As expected, the PEI porous membranes with more PVP contents showed more oblique diffusion curve, indicating poor TEMPO-OH selectivity. The TEMPO-OH permeability of 20PEI/1PVP-z membrane showed lower slopes of diffusion curves, suggesting that the adjustment of THF volatilization time was favorable to improve ion selectivity, which is consistent with the SEM results.

Fig. 4 (d) exhibited the stress-strain curves for different PEI-based porous membranes. The tensile stress of PEI-based porous ion conducting membranes was reduced by adding more PVP content, which was ascribed to the formation of more porous structures. The 20PEI/1PVP achieved breaking stress of 6.84 MPa and elongation at the break of 16.5%. 20PEI/1PVP-z (z = 30s, 60s and 90s) obtained a little higher tensile strain than that of 20PEI/1PVP, where the formation of dense surface layer by volatilizing THF facilitated to improve mechanical stability.

Combining the good selectivity and ion conductivity, the 20PEI/1PVP-90s was further evaluated as a membrane in neutral aqueous Zn/TEMPO-OH flow battery. The TEMPO-based materials are used as cathode in aqueous and non-aqueous electrolytes owing to their high oxidation potential, fast reaction kinetics, and good electrochemical reversibility. Fig. 5(a–c) exhibited the battery performance at different current densities ranging from 10 mA cm^{-2} to 40 mA cm^{-2}. As shown in Fig. 5 (a), the coulombic efficiency (CE) of a single cell with 20PEI/1PVP-90s increased from 96.3% to 98.7% with current densities increasing. The increasing tendency was obtained when using Nafion 115 as a membrane as well. While the CE of Nafion 115 dramatically dropped at the current density of 40 mA cm^{-2}, which resulted from the abnormally low reversible capacity (See Fig. S2). With the increase of current densities, the voltage efficiency (VE) tended to decline due to higher overpotential and concentration polarization (See Fig. 5(b and c)) [27]. Consequently, the 20PEI/1PVP-90s membrane showed a CE of over 98%, a VE of ~78% and an energy efficiency (EE) of about 77% at a current density of 20 mA cm^{-2}. The discharge capacity of Nafion 115 and 20PEI/1PVP-90s as cycling was demonstrated in Fig. 5 (d). Compared to Nafion 115 membrane, the 20PEI/1PVP-90s exhibited higher discharge capacity and comparable capacity retention, which indicated that the PEI-based porous ion conducting membrane got more excellent ion conductivity and selectivity than Nafion 115. Notably, this conclusion was different from area resistant results, where the Nafion 115 showed a little higher ion conductivity than that of PEI-based porous membranes in the NH_4Cl solution. This result can be explained that the Cl^- ion conductivity was different through Nafion 115 and 20PEI/1PVP-90s membrane. The area resistance is attributed to ion conductivity through membrane, either Cl^- or NH_4^+ conductivity. The Cl^- conduction is necessary to balance gain/loss of electrons during charge-discharge process. For the porous 20PEI/1PVP-90s membrane, Cl^- conductivity is based on pore size exclusion. While the Cl^- conductivity through the Nafion 115 can be hindered due to electrostatic interaction as cycling, which was resistant with the result that the flow

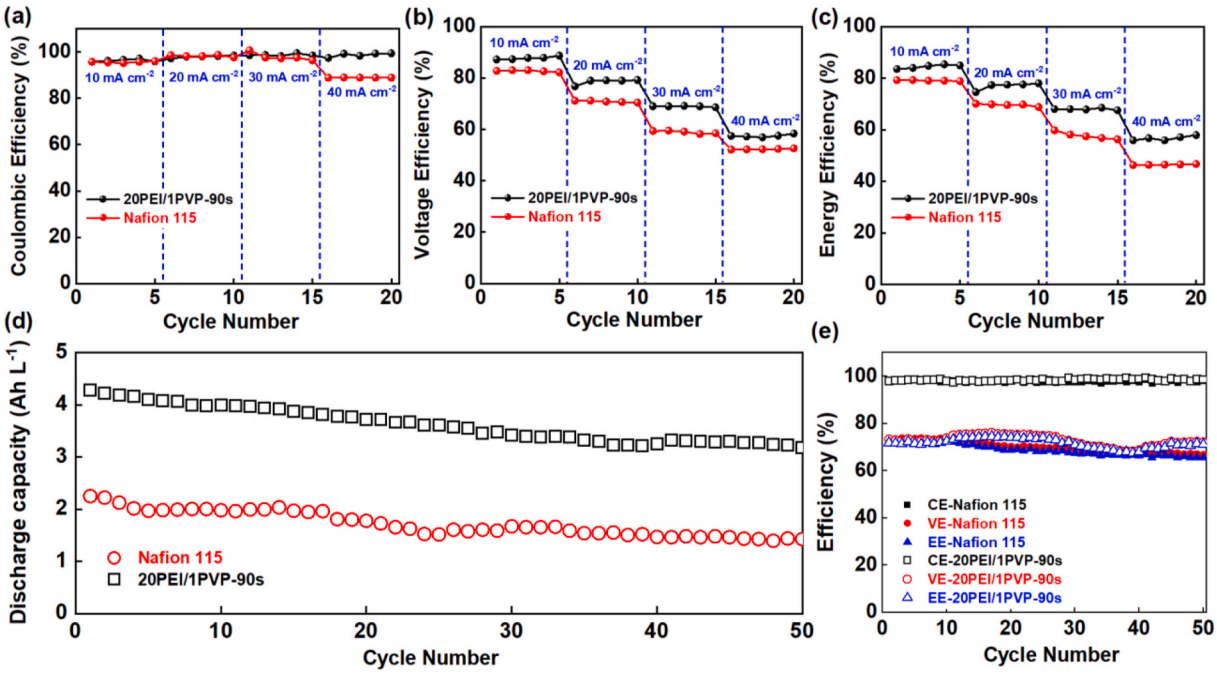

Fig. 5. The Zn/TEMPO-OH flow battery performance of 20PEI/1PVP-90s and Nafion 115 at different current densities: (a) CE, (b) VE, (c) EE; (d) The battery performance of 20PEI/1PVP-90s and Nafion 115 at 20 mA cm^{-2} during 50 cycles; (e) The discharge capacity retention of 20PEI/1PVP-90s and Nafion 115 at 20 mA cm^{-2}.

battery with Nafion 115 delivered lower reversible capacity at 40 mA cm^{-2}. Moreover, the battery assembled with 20PEI/1PVP-90s showed stable performance during over 50 charge-discharge process in Fig. 5 (e), which was comparable to that of Nafion 115.

Table S1 listed the membranes reported in neutral aqueous Zn/TEMPO-based flow batteries. The dialysis membrane (Spectra/Por® 6) and cation exchange membrane (Fumasep® F-930-RFD) were reported for neutral aqueous Zn/TEMPO-based flow batteries [15,16]. Compared to porous dialysis membrane, optimized membrane in this work showed higher selective and ion conductivity. The 20PEI/1PVP-90s showed comparable battery performance to cation exchange membrane, even though slight difference resulted from electrolytes. While compared to cation exchange membrane, 20PEI/1PVP-90s porous membrane obtained more stable cycling performance.

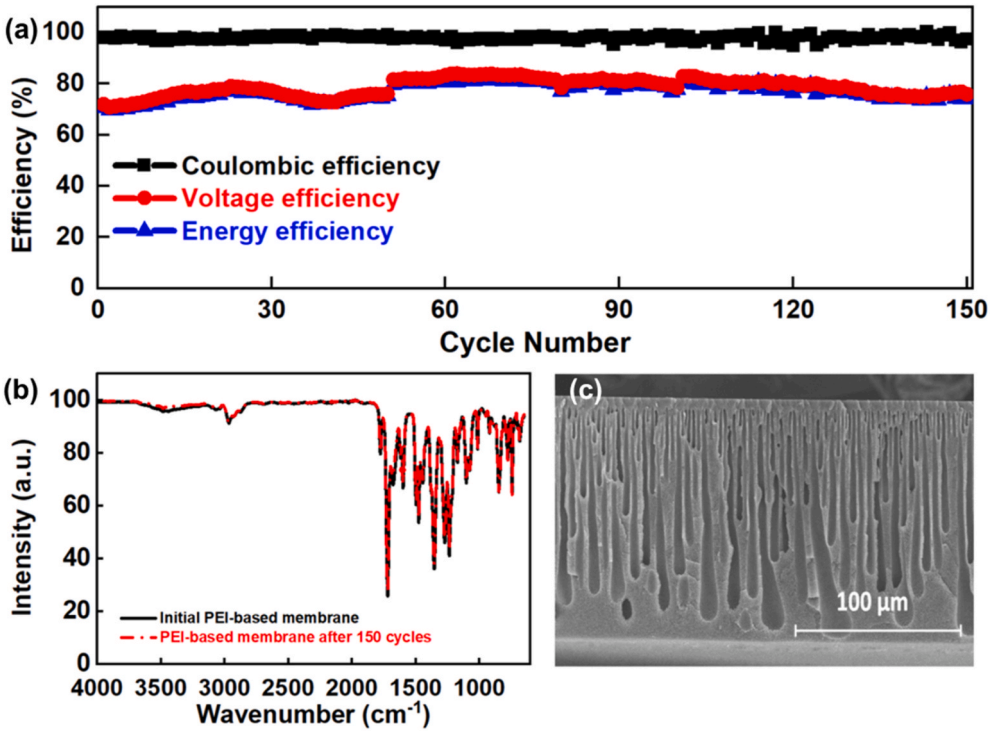

Fig. 6. (a) The cycle performance of 20PEI/1PVP-90s at 20 mA cm^{-2}; (b) The FTIR of 20PEI/1PVP-90s before and after 150 cycles; (c) The SEM images of cross-section of 20PEI/1PVP-90s after 150 cycles.

To investigate the chemical stability of PEI-based porous ion conducting membrane in Zn/TEMPO-OH flow battery, a 20PEI/1PVP-90s membrane was further evaluated in a long-term cycling test at the current density of 20 mA cm^{-2}. The battery exhibited a stable performance after continuously running 150 cycles (See Fig. 6 (a)), which was superior to reported dialysis membrane and cation exchange membrane. The fluctuation of CE in the long-term cycling test is attributed to the changes in atmosphere temperature during charge-discharge proceeding. The battery capacity retention during 150 cycles was shown in Fig. S3. The electrolytes in positive and negative tanks were replaced after every 50 cycles test, which minimized the effect of electrolyte side reactions on battery performance. In the test period (50 cycles), the flow battery with 20PEI/1PVP-90s exhibited over 70% capacity retention. The chemical structure of the membrane before and after long-term cycling was characterized through Fourier transform infrared spectroscopy (FTIR). In Fig. 6 (b), the similar FTIR spectra were obtained before and after cycling, and no new peaks were observed, indicating that the PEI-based porous membrane maintained good chemical stability in Zn/TEMPO-OH flow battery [28]. Fig. 6 (c) showed the cross-section morphology of 20PEI/1PVP-90s after 150 cycles. Compared to the initial 20PEI/1PVP-90s membrane (See Fig. 2 (i)), the cross-section morphologies of 20PEI/1PVP-90s membrane after long-term cycling rarely changed, further demonstrating outstanding chemical stability of PEI-based porous ion conducting membrane.

3. Conclusions

To address poor ion conductivity and stability of ion exchange membrane in ZFBs, PEI-based porous membranes were fabricated and developed by water phase inversion technology, and optimized via adjusting the amount of PVP in a cast solution and controlling volatilization time of co-solvent THF before phase separation. The introduction of PVP is favorable to form connected porous structure, and then a dense skin layer is constructed via adding THF and extending the THF volatilization time before phase separation. Consequently, the optimized PEI-based membrane, 20PEI/1PVP-90s membrane, showed excellent battery performance in neutral aqueous Zn/TEMPO-OH flow battery. The flow battery with 20PEI/1PVP-90s achieved a CE of over 98%, a VE of ~78% and an EE of about 77% and stably ran for 150 cycles at the current density of 20 mA cm^{-2}, which is superior to the reported membranes in neutral aqueous Zn/-TEMPO-based flow battery. The development of PEI-based porous ion conducting membranes provides a promising substitute for commercial CEM (like Nafion 115 membrane) and paves a new pathway for developing highly effective and low cost ZFBs.

4. Experimental

4.1. Materials

Polyetherimide (PEI, Sigma-Aldrich), 1-Methyl-2-pyrrolidinone (NMP, ≥99%, Sigma-Aldrich), polyvinylpyrrolidone (M.W. 40000, Alfa Aesar), ammonium chloride (≥99.5%, Sigma-Aldrich), 4-Hydroxy-2,2,6,6-tetramethyl-piperidine 1-Oxyl (TEMPO-OH, >98.0%, TCI), anhydrous zinc chloride (>98%, Alfa Aesar) and anhydrous tetrahydrofuran (≥99.8%, Alfa Aesar) were used as received. High purity zinc foil (99.9%, thickness of 200 μm, Micro Trader) and dried loofah sponge (MAYMII·HOME) were used as received. Nafion N115 was ordered from Ion Power Inc.

4.2. Fabrication of membranes

The cast solution was prepared from PEI and different weight ratios of PVP in the NMP and then the solution was mixed and heated at 120 °C for 5 h to form the homogenous solution. The total weight concentration of polymer in a cast solution was kept in 25 wt%. The cast solution was referred as xPEI/yPVP, where x/y was the weight ratio of PEI to PVP. The polymer solution was cast on a dust-free glass plate at room temperature with the related humidity of less than 40%. To future improve the selectivity of porous membrane, the THF of 10 wt% of total solvent was added into the 20PEI/1PVP solution as co-solvent. The various volatilization time was tuned before the membrane casted polymer solution was immersed in the water. The prepared membranes were named as 20PEI/1PVP-z, which z stands for the volatilization time. The prepared membrane was stored in the deionized water at room temperature and was treated by immersing in 1 M ammonium chloride solution for 24 h before use.

4.3. Membrane characterization

4.3.1. Scanning electronic microscopy (SEM)

The surface and cross-section morphologies of prepared membrane were observed using scanning electron microscope (S4800, Hitachi). The membranes were soaked in ethanol for 24 h before imaging to remove dust from the atmosphere. The cross-section of samples was observed by breaking the membranes in liquid nitrogen. All samples were platinum coated before use.

4.3.2. Contact angle measurements

The static contact angle was investigated using an optical contact angle measuring instrument (SDC-350, SINDIN). The membranes were dried at 60 °C for 48 h to remove water from the membrane and taped on a glass substrate before measurement. A frozen image was captured after 5 μL deionized water was dropped on the flat membrane surface for 5 s.

4.3.3. Water uptake and porosity

A prepared membrane with 1.37 square inch was immersed in the water for 24 h, then quickly wiped out the water on the surface. The weight, thickness and area of wet membrane were measured, and then the dried membrane was dried in vacuum oven at 60 °C for 48 h to remove water from the membrane. Then the weight of dried membranewas measured immediately to avoid the effect of water vapor in the atmosphere. The water uptake is calculated by equation (1):

$$\text{Water Uptake} = \left[\frac{(W_{wet} - W_{dry})}{W_{dry}}\right] \times 100\ \% \quad (1)$$

Where the W_{wet} and W_{dry} stand for the weight of wet and dried membrane, respectively.

The porosity of membranes can be calculated by equation (2):

$$\text{Porosity} = \left[\frac{(W_{wet} - W_{dry})/\rho}{A \times d}\right] \times 100\% \quad (2)$$

where ρ is the water density at room temperature, A is the effective area of membrane, and d is the thickness of membrane.

4.3.4. Membrane swelling

The prepared membrane with 1.37 square inch was immersed in water for 24 h. The length of the wet membrane was recorded as L_{wet}. The membrane was dried in vacuum oven at 80 °C for 48 h to completely remove water from the membrane and measure the length of the dry membrane on the same side, recorded as L_{dry}. The swelling ratio is calculated by equation (3):

$$\text{Membrane Swelling} = \left[\frac{(L_{wet} - L_{dry})}{L_{dry}}\right] \times 100\% \quad (3)$$

4.3.5. Tensile strength

The tensile strength of wet membrane was measured by a rotational rheometer (ARES-G2, TA Instruments). The samples were cut into the size of 30 mm in length and 1 mm in width and stored in water until the measurements. 80 μm min^{-1} displacement speed and 50 N maximum

load cell were applied during characterization.

4.3.6. Area resistance and ion conductivity measurements

The area resistance of membranes was measured in a flow cell by electrochemical impedance spectroscopy (EIS) with the sinusoidal voltage waveform of amplitude 10 mV (SP-150, BioLogic). The frequency range is from 100 kHz to 100 mHz. A flow cell with an effective area of 5 cm^2 (2.3×2.2 cm^2) was assembled with 1 M NH_4Cl as electrolytes.

The EIS was measured with and without the membranes to calculate the area resistance by using equation (4):

$$R_A = (R_2 - R_1) \times A \quad (4)$$

Where R_1 is the cell resistance without membrane, R_2 is the cell resistance with membrane. A is the effective area.

The ionic conductivity can be calculated by equation (5):

$$\sigma = \frac{d}{(R_2 - R_1) \times A} \quad (5)$$

Where d was the thickness of the wet membrane.

4.3.7. TEMPO-OH permeability

The selectivity of a membrane is evaluated by TEMPO-OH permeability. A membrane was assembled in a H-cell of 20 mL, where an 8 mL 0.2 M TEMPO-OH in 0.2 M $ZnCl_2$ and 1 M NH_4Cl solution and an 8 mL 0.2 M $ZnCl_2$ in 1 M NH_4Cl solution were filled in left and right half-cell, respectively. The solutions in both half-cell were vigorously stirred to minimize concentration polarization. A 2 mL solution was collected at a regular interval and the concentration of TEMPO-OH in the sample solution was detected via UV–Visible spectrophotometer (V770, Jasco).

4.3.8. Flourier transformed infrared spectroscopy (FTIR)

The chemical structure of the membranes was characterized using an Agilent Cary 630 spectrometer. Each spectrum was recorded at a rate of 32 scans with a resolution of 4 cm^{-1}, collected from 650 to 4000 cm^{-1} in transmittance mode.

4.4. Single flow battery performance

Similar to our previous published work, the Zn-TEMPO-OH flow battery was assembled by sandwiching a membrane between graphite felts (cathode) and zinc foil (anode), clamped by two pieces of graphite flow fields and gold coating current collectors. All the parts were fixed between two stainless steel endplates. The effective area of the electrode and membrane was ~5 cm^2. 10 mL of the positive and negative electrolytes was filled in each flow tank, as driven by peristaltic pumps (Masterflex L/S, Cole-Parmer) with a 40 mL min^{-1} flow rate. The graphite felt (GFD 4, 6 EA, Sigracell) was treated at 400 °C for 30 h in the air, and two pieces of graphite felts were used as electrode in each side. The dried loofah sponge was cut in 2.3×2.2 cm^2 and used in anode side as supporting frame to fix Zn foil. The Nafion 115 was rinsed with water and stored in the 1 M ammonium chloride solution for 24 h before use. The cycling and rate performance were carried out by a battery test system (CT2001A, LAND, China) under constant current densities, and the cutoff voltage for the charge and discharge process was between 0.8 V and 2 V.

Declaration of competing interest

The authors declare that they have no known competing financial interests or personal relationships that could have appeared to influence the work reported in this paper.

Acknowledgment

The authors acknowledge the use of SEM facility under the auspices of Northeastern University Center for Renewable Energy technology (NUCRET).

Appendix A. Supplementary data

Supplementary data to this article can be found online at https://doi.org/10.1016/j.memsci.2021.119804.

References

[1] Z. Yang, J. Zhang, M.C. Kintner-Meyer, X. Lu, D. Choi, J.P. Lemmon, J. Liu, Electrochemical energy storage for green grid, Chem. Rev. 111 (2011) 3577–3613.
[2] Y. Yang, X. Sun, Z. Cheng, A. Mukhopadhyay, A. Natan, C. Liu, D. Cao, H. Zhu, Functionalized well-aligned channels derived from wood as a convection-enhanced electrode for aqueous flow batteries, ACS Appl. Energy Mater. 3 (2020) 6249–6257.
[3] C. Ding, H. Zhang, X. Li, T. Liu, F. Xing, Vanadium flow battery for energy storage: prospects and challenges, J. Phys. Chem. Lett. 4 (2013) 1281–1294.
[4] A. Mukhopadhyay, Y. Yang, Y. Li, Y. Chen, H. Li, A. Natan, Y. Liu, D. Cao, H. Zhu, Mass transfer and reaction kinetic enhanced electrode for high-performance aqueous flow batteries, Adv. Funct. Mater. 29 (2019).
[5] C. Xie, H. Zhang, W. Xu, W. Wang, X. Li, A long cycle life, self-healing zinc-iodine flow battery with high power density, Angew. Chem. 57 (2018) 11171–11176.
[6] W. Lu, C. Xie, H. Zhang, X. Li, Inhibition of zinc dendrite growth in zinc-based batteries, ChemSusChem 11 (2018) 3996–4006.
[7] B. Li, Z. Nie, M. Vijayakumar, G. Li, J. Liu, V. Sprenkle, W. Wang, Ambipolar zinc-polyiodide electrolyte for a high-energy density aqueous redox flow battery, Nat. Commun. 6 (2015) 6303.
[8] X. Li, H. Zhang, Z. Mai, H. Zhang, I. Vankelecom, Ion exchange membranes for vanadium redox flow battery (VRB) applications, Energy Environ. Sci. 4 (2011) 1147–1160.
[9] W. Lu, Z. Yuan, Y. Zhao, H. Zhang, H. Zhang, X. Li, Porous membranes in secondary battery technologies, Chem. Soc. Rev. 46 (2017) 2199–2236.
[10] R. Tan, A. Wang, R. Malpass-Evans, R. Williams, E.W. Zhao, T. Liu, C. Ye, X. Zhou, B.P. Darwich, Z. Fan, L. Turcani, E. Jackson, L. Chen, S.Y. Chong, T. Li, K.E. Jelfs, A.I. Cooper, N.P. Brandon, C.P. Grey, N.B. McKeown, Q. Song, Hydrophilic microporous membranes for selective ion separation and flow-battery energy storage, Nat. Mater. 19 (2020) 195–202.
[11] Q. Dai, Z. Liu, L. Huang, C. Wang, Y. Zhao, Q. Fu, A. Zheng, H. Zhang, X. Li, Thin-film composite membrane breaking the trade-off between conductivity and selectivity for a flow battery, Nat. Commun. 11 (2020) 13.
[12] A. Mukhopadhyay, Y. Yang, Z. Cheng, P. Luan, A. Natan, H. Zhu, Proton-conductive membranes with percolated transport paths for aqueous redox flow batteries, Materials Today Nano 13 (2021).
[13] A. Mukhopadhyay, Z. Cheng, A. Natan, Y. Ma, Y. Yang, D. Cao, W. Wang, H. Zhu, Stable and highly ion-selective membrane made from cellulose nanocrystals for aqueous redox flow batteries, Nano Lett. 19 (2019) 8979–8989.
[14] W. Xu, Y. Zhao, Z. Yuan, X. Li, H. Zhang, I.F.J. Vankelecom, Highly stable Anion exchange membranes with internal cross-linking networks, Adv. Funct. Mater. 25 (2015) 2583–2589.
[15] J. Winsberg, C. Stolze, A. Schwenke, S. Muench, M.D. Hager, U.S. Schubert, Aqueous 2,2,6,6-tetramethylpiperidine-N-oxyl catholytes for a high-capacity and high current density oxygen-insensitive hybrid-flow battery, ACS Energy Letters 2 (2017) 411–416.
[16] J. Winsberg, T. Janoschka, S. Morgenstern, T. Hagemann, S. Muench, G. Hauffman, J.F. Gohy, M.D. Hager, U.S. Schubert, Poly(TEMPO)/Zinc hybrid-flow battery: a novel, "green," high voltage, and safe energy storage system, Adv. Mater. 28 (2016) 2238–2243.
[17] H. Zhang, H. Zhang, X. Li, Z. Mai, J. Zhang, Nanofiltration (NF) membranes: the next generation separators for all vanadium redox flow batteries (VRBs)? Energy Environ. Sci. 4 (2011) 1676–1679.
[18] H. Zhang, H. Zhang, X. Li, Z. Mai, W. Wei, Silica modified nanofiltration membranes with improved selectivity for redox flow battery application, Energy Environ. Sci. 5 (2012) 6299–6303.
[19] I.M. Wienk, R.M. Boom, M.A.M. Beerlage, A.M.W. Bulte, C.A. Smolders, H. Strathmann, Recent advances in the formation of phase inversion membranes made from amorphous or semi-crystalline polymers, J. Membr. Sci. 113 (1996) 361–371.
[20] Y. Li, H. Zhang, X. Li, H. Zhang, W. Wei, Porous poly (ether sulfone) membranes with tunable morphology: fabrication and their application for vanadium flow battery, J. Power Sources 233 (2013) 202–208.
[21] J. Cao, H. Zhang, W. Xu, X. Li, Poly(vinylidene fluoride) porous membranes precipitated in water/ethanol dual-coagulation bath: the relationship between morphology and performance in vanadium flow battery, J. Power Sources 249 (2014) 84–91.
[22] L. Qiao, H. Zhang, W. Lu, C. Xiao, Q. Fu, X. Li, I.F.J. Vankelecom, Advanced porous membranes with slit-like selective layer for flow battery, Nanomater. Energy 54 (2018) 73–81.

[23] M. Shi, Q. Dai, F. Li, T. Li, G. Hou, H. Zhang, X. Li, Membranes with well-defined selective layer regulated by controlled solvent diffusion for high power density flow battery, Advanced Energy Materials 10 (2020).
[24] J.-H. Kim, K.-H. Lee, Effect of PEG additive on membrane formation by phase inversion, J. Membr. Sci. 138 (1998) 153–163.
[25] R.M. Boom, T. van den Boomgaard, C.a. Smolders, Mass transfer and thermodynamics during immersion precipitation for a two-polymer system: evaluation with the system PES—PVP—NMP—water, J. Membr. Sci. 90 (1994) 231–249.
[26] T.T. Chau, W.J. Bruckard, P.T. Koh, A.V. Nguyen, A review of factors that affect contact angle and implications for flotation practice, Adv. Colloid Interface Sci. 150 (2009) 106–115.
[27] Y. Zhao, M. Li, Z. Yuan, X. Li, H. Zhang, I.F.J. Vankelecom, Advanced charged sponge-like membrane with ultrahigh stability and selectivity for vanadium flow batteries, Adv. Funct. Mater. 26 (2016) 210–218.
[28] Y. Zhao, W. Lu, Z. Yuan, L. Qiao, X. Li, H. Zhang, Advanced charged porous membranes with flexible internal crosslinking structures for vanadium flow batteries, J. Mater. Chem. 5 (2017) 6193–6199.